International Journal of GEOMATE, March, 2026 Vol.30, Issue 139, pp.22-37
ISSN: 2186-2982 (P), 2186-2990 (O), Japan, DOI: https://doi.org/10.21660/2026.139.5234
Geotechnique, Construction Materials and Environment

HYDROLOGICAL DYNAMICS AND IMPACTS IN THE PEATLAND WATERSHED OF SOUTH SUMATRA, INDONESIA

*Mokhamad Yusup Nur Khakim[1,2], Azhar Kholiq Affandi[1,2], Muhammad Irfan[1] and Erni[1]

[1]Physics Department, Mathematics and Natural Science Faculty, Universitas Sriwijaya, Indonesia; [2]Physics Graduate Program, Mathematics and Natural Science Faculty, Universitas Sriwijaya, Indonesia

*Corresponding Author, Received: 19 Sep. 2025, Revised: 08 Nov. 2025, Accepted: 10 Nov. 2025

ABSTRACT. Climate change and human activities, such as El Niño, agricultural drainage, and deforestation, have caused hydrological problems in peatlands. This study employed remote sensing to assess hydrological dynamics, variations in the moisture stress index, and vegetation health in the peatland watershed of the Sugihan–Saleh Peat Hydrological Unit from 2005 to 2024. Hydrological modelling, utilizing the Soil Conservation Service Curve Number approach, revealed variations in surface runoff and water storage across land cover types. The study area experienced a significant water deficit during El Niño events. Furthermore, reducing tree cover during these extreme drought seasons led to increased runoff in the following years. Due to restoration activities, the area of bare land/sparse vegetation decreased slightly from 37.69 ha in 2015 to 28.42 ha in 2024. Tree cover generally increased from 3,932.67 ha in 2015 to 7,646.74 ha in 2024, improving soil infiltration and lowering runoff. Bare land/sparse vegetation contributed the most to surface runoff, 29%. In contrast, the area of tree cover, dominated by peat forest, had the lowest runoff contribution (6.6%) and the highest storage capacity. The study highlights the moisture retention in tree-covered areas, with surpluses in rainy seasons and deficits in dry seasons, particularly during El Niño events. Conservation areas show better moisture conditions and better water resource management. Long-term monitoring and modifying cultivation practices are needed for peatland sustainability.

Keywords: Peatland, Hydrology, Water balance, Runoff, Restoration

1. INTRODUCTION

Peatlands contribute to biodiversity and ecological balance, but they are threatened due to hydrological disturbances. Typically, peat fires were caused by drainage practices used for agriculture and plantations, resulting in severe soil moisture reductions [1]. Additionally, natural factors like low rainfall during the dry seasons often worsen drought conditions. During extreme droughts, hydrological imbalances impact local communities and ecosystems by increasing fire vulnerability, destroying biodiversity, producing hazardous smoke, and impairing public health and livelihoods. When combined with the common practice of burning to clear land, these factors lead to a catastrophic cycle that is still challenging to overcome.

Indonesia holds about 13.4 Mha of tropical peatlands, the largest global carbon stock [2, 3]. The peatlands are significant for Indonesia's ambition to become net-zero for GHGs by 2060, and therefore, peatland conservation and restoration are a national climate change mitigation requirement [4].

Peatland burning not only leads to habitat and biodiversity loss but also to carbon emissions, contributing to global climate change [5–7]. Between July and October 2015, Indonesian peat fires emitted an estimated 0.002 Gt, consisting of 81% CO_2, 16% CO, and 2.3% CH_4 [8]. Accelerated warming in boreal regions could substantially increase in carbon emissions from peat wildfires, escalating from 143 Mt in 2015 to 544 Mt by 2100, with a cumulative total of 28 Gt for the 21st century [9]. These consequences encompass health issues arising from air pollution and economic losses for communities dependent on peatlands [10, 11]. Therefore, a comprehensive understanding of the causes and consequences of peatland fires is crucial for developing suitable mitigation strategies for this important ecosystem.

Mitigating catastrophic fires in tropical peatlands depends extensively on remote sensing and geographical information systems (GIS) [12], especially for assessing hydrological conditions [13]. For example, remote sensing of soil moisture and water level changes in peatlands is a key tool for monitoring fire susceptibility [14, 15]. Satellite data enable the identification of areas with reduced moisture and provide advanced warnings of high fire risk [16–18]. Remote sensing and GIS offer the capacity to create large-scale descriptions of hydrological dynamics [13, 19]. Understanding hydrological conditions is necessary for planning and restoration initiatives that aim to maintain ecosystem sustainability [2, 20, 21].

Hydrological modelling tools such as SWAT and HEC-HMS [22] have been developed to simulate the water cycle in watersheds. These models are commonly used to assess hydrological imbalance, known as disturbances in natural water balance due to detailing interactions between evapotranspiration variability, precipitation, runoff variability, infiltration, and runoff-evapotranspiration.

Alternatively, hydraulic degradation defines the structure and conduction capacity loss of hydraulic structures such as embankments, channels, or dams. Hydraulic degradation has the potential to modify flow behavior and increase flood risk. Hydrodynamic behaviors were examined for zoned earth dams under earthquake loads [23]. In addition, dam failure and flood wave propagation were modeled using 2D HEC-RAS [24, 25]. Such analyses provide evidence for hydraulic degradational processes, which are fundamentally different from hydrological imbalance in natural peatlands.

Advanced models like HEC-HMS and SWAT give realistic simulations of the watershed processes; they still need heavy input data and calibration to simulate realistically the condition of the watersheds [26, 27]. Their complexity makes them resource-intensive and time-consuming, with a greater risk of reduced precision if data quality is poor.

The Soil Conservation Service Curve Number (SCS-CN) technique [28, 29] is a practical alternative, particularly for watersheds with limited data. The SCS-CN model is widely used for its simplicity and reliability, requiring only three main inputs, including land cover, hydrological soil group, and rainfall [30]. It is particularly valuable where resources are limited, enabling feasible and rapid runoff estimation for watersheds.

This study analyzed the relationship between surface runoff, water storage change, moisture stress index, and enhanced vegetation index from 2005 to 2024, emphasizing the effects of extreme climate events such El Niño and La Niña. Integrating vegetation and hydrology, the study investigates ecosystem responses to climatic anomalies, with annual land cover classification used to enhance runoff modeling accuracy. Ultimately, this study aims to assess the effectiveness of restoration programs in rehabilitating hydrological processes and post-restoration vegetation under long-term climate variability.

2. RESEARCH SIGNIFICANCE

This study offers valuable information about the hydrological functioning of peatland ecosystems under climate variability and human perturbations. Through remote sensing and hydrologic modeling, the study illustrates the impact of deforestation and restoration on land cover change on runoff, water storage, and moisture stress. The results highlight the susceptibility of peatlands to droughts caused by El Niño and the role of conservation and restoration in improving the regulation of water. These findings are important to inform long-term planning for peatland restoration and sustainable land management.

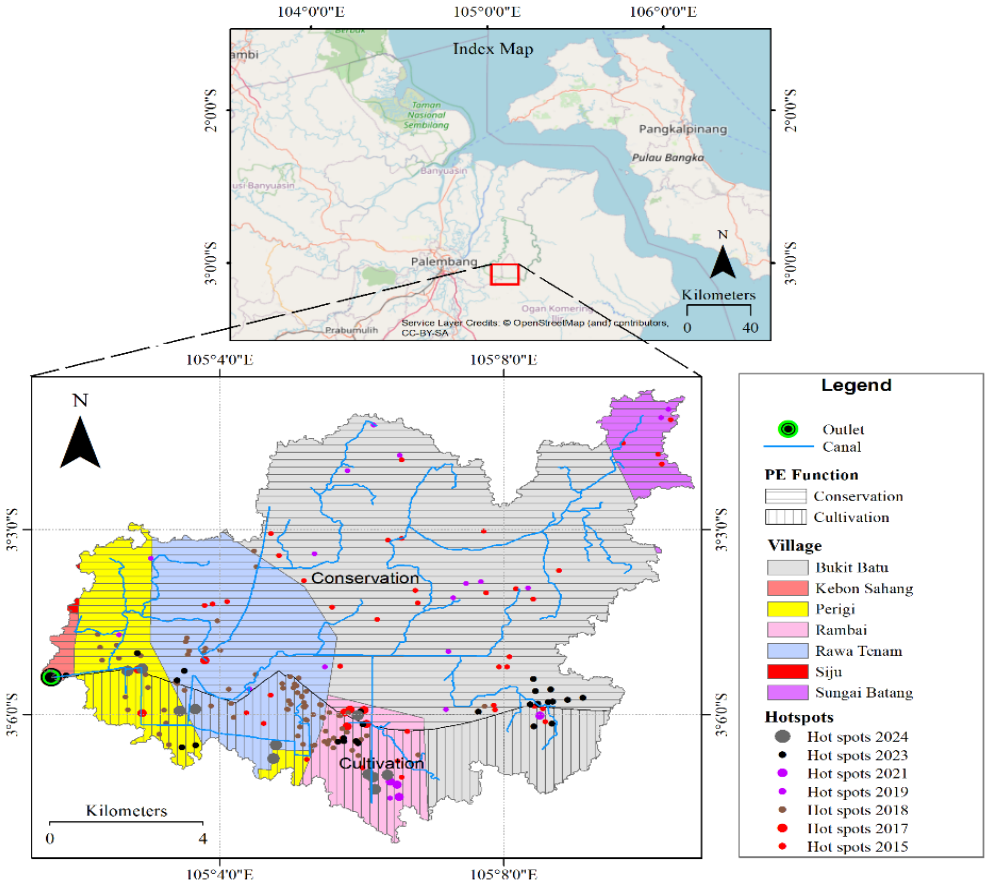

Fig. 1. Overview of the study area

3. MATERIALS AND METHODS

3.1 Study Area

The study area is located in the Sugihan–Saleh Rivers Peat Hydrological Unit, South Sumatra, Indonesia (Figure 1), covering 12,879 ha and including seven villages. The peat ecosystem (PE) function is divided into a conservation area in the north (2,960 ha) and a cultivation area in the south (9,862 ha). El Niño 2015 significantly enhanced subsidence and vegetation degradation in this area [31]. The hotspots distribution shows the distribution of the fires that took place in 2015, and the distribution was dispersed in 2019. Meanwhile, in the case of the 2023 fires, it was concentrated around the ecosystem function border, with the most hotspots happening within Bukit Batu Village.

Following severe fires in 2015, this region became a focus for peatland restoration between 2016 and 2020. The restoration in the present study means rehabilitation of peatland with the application of the 3R principle: Rewetting, Revegetation, and Revitalization. Dominant in the study site is rewetting, and it is predominantly executed through plugging the canals to increase and stabilize the groundwater level. Rehabilitation has attempted to enhance livelihood within the local community by encouraging off-conserve peat land use for small-scale agriculture, mitigating the anthropogenic load on the central peat ecosystem. Revegetation takes place only at a limited scale as demonstration plots to encourage natural regeneration. Long-term hydrological monitoring is vital to evaluate restoration impacts and responses to climate extremes.

3.2 Methods

A flowchart of the entire research process appears in Figure 2. The chart gives a glimpse of the association between the datasets and steps of analysis, allowing for comprehension of the methodological framework, which is discussed in detail in the succeeding sub-sections of the method. All remote sensing datasets utilized in this study were accessed directly from Google Earth Engine (GEE), which provides petabyte-scale access to a wide variety of public and analysis-ready datasets.

3.2.1 Land cover classification

Land cover was classified using Landsat-7 and Landsat-8 imagery (2005 – 2024) processed in the Google Earth Engine (GEE). Surface reflectance data were atmospherically corrected and masked for clouds and shadows. The Landsat-7 image gap caused by the scanline error was removed.

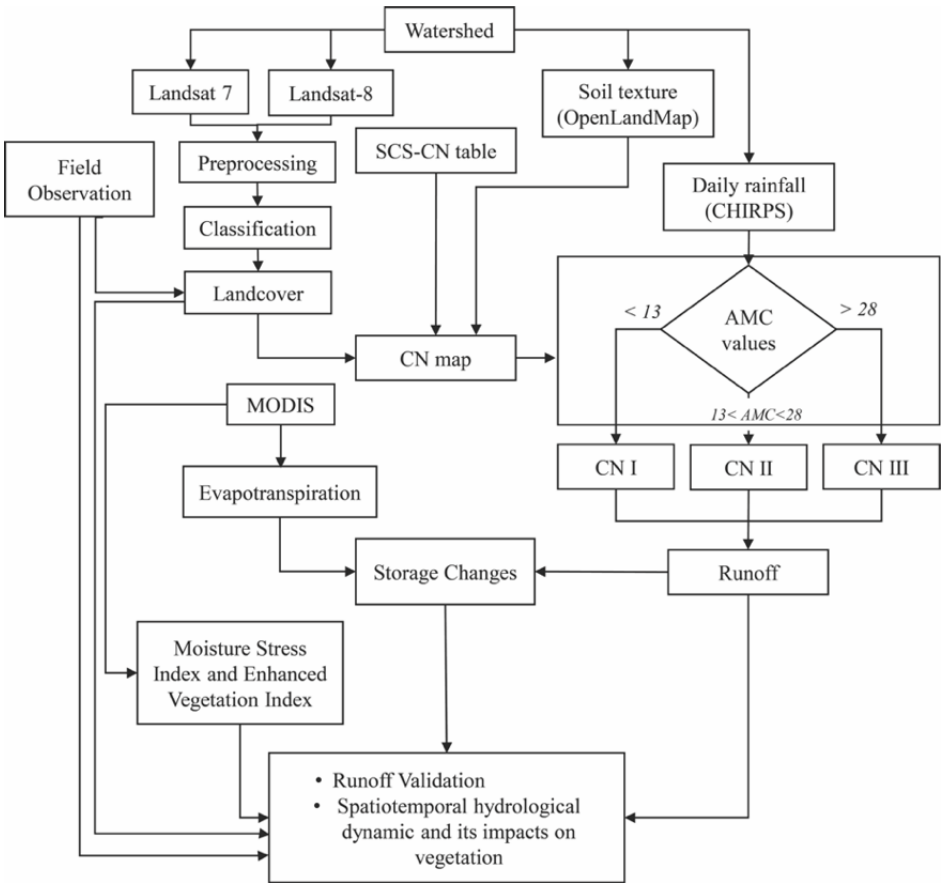

Fig. 2. Flowchart of the study workflow

Median composite images consisting of six bands, i.e., SR_B1-B5, SR_B7 for Landsat-7 (2005 – 2012) and SR_B2-B7 for Landsat-8 (2013 – 2024) were used as the input datasets in the random forest (RF) classification. Additionally, we also integrated derived indices and spectral fractions derived from the Landsat imagery into the input composite. The indices consisted of NDVI, NDWI, and NDBI, and the spectral fractions were Soil, Green Vegetation, Non-Photosynthetic Vegetation, Shade-normalized Green Vegetation, Shade, and Normalized Difference Fraction Index to enhance classification.

Training samples derived from visual inspection of satellite composites were verified through field observations to produce a total of 541 reference points representative of major land cover classes in the reference year, 2020. The land cover classes consist of tree covers, shrubland, grassland, cropland, built-up, bare/sparse vegetation, and water bodies. Land cover classification followed a scheme modified from the ESA WorldCover 10 m classification system [32]. The dataset was aggregated into seven major land cover classes to surface dominance in the study area. The tree cover class contains both peat forest and managed plantation covers, which may comprise oil palm and rubber. These two vegetation types, however, vary in canopy interception, rooting depth, and hydrological response, but were still maintained under one unified class definition for consistency purposes and to further reduce subjective reclassification.

The training samples were, therefore, migrated to each target year, from 2005 through 2024, based on the spectral distance threshold (SDT). A SED (squared Euclidean distance) metric in the GEE environment was used to quantify the spectral similarity of corresponding pixels in the reference and target composite for all selected bands and indices. Samples whose SED values were below the threshold were kept as representative training data for that particular target year.

In this process, a separate RF model was trained for each year, using the split of migrated samples into 70% for training and 30% for validation. From the set of candidate values, the SDT and RF hyperparameters, i.e., number of trees (nTree), number of variables per split (varperSplit), the bag fraction (bagFr), the maximum number of leaf nodes (maxLf), and the seed, were sequentially tuned to provide the highest overall accuracy. This adaptive approach lets each annual model capture interannual spectral variability resulting from atmospheric, sensor, and phenological differences, leading to more reliable multi-year land cover classifications than a fixed-reference-year model. The SDT, the number of migrated samples (NMS), and the RF hyperparameter as presented in Table 1. SDT and NMS variations show that the spectrum changes over time, whereas adaptive RF hyperparameters show that the model is more complicated in years with more spectral variability. An example presented in Figure 3 was used to choose optimum parameter values (red dot) for the 2017 land cover classification consisting of the number of decision tree (120), the number of variable split (6), the bag fraction (0.5), the minimum leaf population (1), the maximum number of leaf nodes (50), and the seed (281).

Table 1. Spectral distance thresholds and optimum RF parameters with the minimum leaf population 1

Year	SDT	NMS	nTree	varperSplit	bagFr	maxLf	seed
2005	0.4	508	160	3	0.60	60	46
2006	0.2	327	60	4	0.50	40	171
2007	0.2	455	120	3	0.35	40	171
2008	0.2	472	170	2	0.50	50	161
2009	0.5	516	160	4	0.50	50	371
2010	1.0	526	140	3	0.65	80	151
2011	0.7	508	20	4	0.50	70	91
2012	0.1	392	140	3	0.50	40	331
2013	1.8	538	100	8	0.50	40	311
2014	0.4	513	140	4	0.45	50	71
2015	0.7	521	190	3	0.50	70	201
2016	0.6	530	20	3	0.50	50	151
2017	0.8	526	120	6	0.50	50	281
2018	0.3	484	170	3	0.50	50	191
2019	0.3	460	110	3	0.50	50	381
2020	ref	541	40	7	0.65	40	181
2021	0.7	527	40	7	0.65	40	181
2022	0.1	459	160	2	0.45	60	121
2023	2.0	533	150	9	0.50	50	341
2024	0.1	418	20	3	0.45	50	21

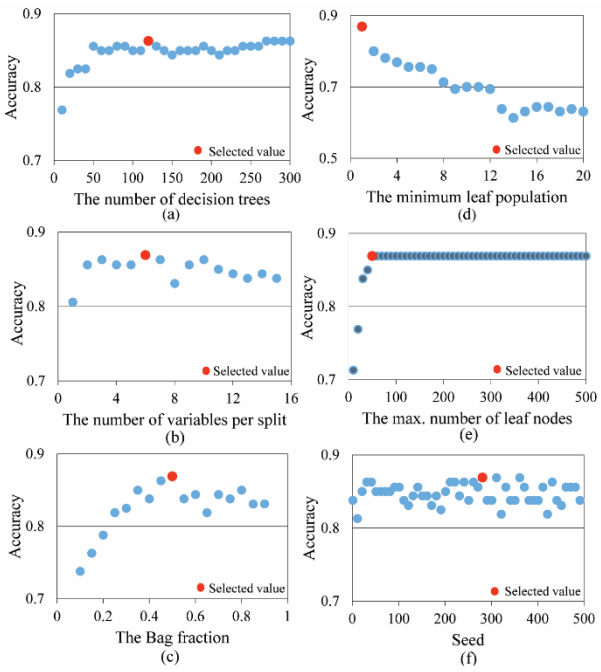

Fig. 3. Example charts for selecting the optimal parameter values in the random forest classification for the 2017 land cover

Table 2. Accuracy measures for land cover classification

Year	OA	Kappa	Tree cover		Shrubland		Grassland		Cropland		Built-up		Bare/sparse vegetation		Water Body	
			PA	UA	PA	UA	PA	UA	PA	UA	PA	UA	PA	UA	PA	UA
2005	0.79	0.73	0.84	0.75	0.67	0.70	0.70	0.78	0.73	0.80	1.00	0.94	0.80	1.00	0.83	0.83
2006	0.83	0.75	0.93	0.84	0.53	0.77	0.88	0.78	1.00	0.86	0.75	1.00	0.50	1.00	1.00	1.00
2007	0.80	0.73	0.80	0.82	0.58	0.56	0.76	0.76	0.88	0.88	1.00	1.00	0.00	0.00	1.00	0.90
2008	0.83	0.78	0.91	0.79	0.65	0.89	0.77	0.85	1.00	0.75	1.00	1.00	0.80	1.00	1.00	0.75
2009	0.83	0.78	0.90	0.80	0.62	0.68	0.69	0.88	0.93	0.88	0.94	0.89	0.91	0.91	0.83	1.00
2010	0.80	0.73	0.92	0.81	0.71	0.75	0.50	0.76	0.83	0.71	0.94	0.89	1.00	0.71	0.67	1.00
2011	0.78	0.72	0.86	0.73	0.47	0.78	0.77	0.79	0.82	1.00	0.89	0.76	0.56	0.83	0.89	0.80
2012	0.85	0.80	0.85	0.87	0.65	0.73	0.88	0.77	0.80	1.00	1.00	1.00	0.00	0.00	1.00	1.00
2013	0.89	0.86	0.95	0.87	0.78	0.91	0.82	0.88	1.00	0.82	0.87	1.00	1.00	0.90	1.00	1.00
2014	0.81	0.76	0.91	0.73	0.53	0.82	0.76	0.84	0.71	0.83	0.96	0.85	0.87	0.87	0.92	1.00
2015	0.82	0.77	0.81	0.90	0.75	0.64	0.69	0.69	0.80	1.00	1.00	0.89	1.00	0.85	1.00	1.00
2016	0.89	0.87	0.93	0.92	0.79	0.76	0.81	0.96	1.00	0.84	1.00	0.95	0.80	1.00	0.89	0.80
2017	0.87	0.84	0.87	0.92	0.73	0.76	0.92	0.85	0.88	0.78	1.00	0.83	0.78	1.00	1.00	0.92
2018	0.84	0.79	0.91	0.82	0.65	0.81	0.89	0.74	0.22	1.00	1.00	1.00	1.00	1.00	1.00	1.00
2019	0.86	0.82	0.91	0.89	0.76	0.68	0.77	0.85	0.83	1.00	1.00	0.92	0.50	1.00	1.00	1.00
2020	0.88	0.85	0.85	0.87	0.72	0.84	0.89	0.82	0.89	0.80	1.00	0.95	0.93	0.93	1.00	1.00
2021	0.93	0.91	0.88	1.00	1.00	0.73	0.93	0.90	0.88	1.00	1.00	1.00	1.00	1.00	1.00	1.00
2022	0.85	0.80	0.94	0.81	0.55	1.00	0.79	0.79	0.89	0.89	1.00	0.94	0.80	0.80	1.00	1.00
2023	0.83	0.79	0.84	0.91	0.67	0.78	0.88	0.69	0.93	0.93	0.88	0.94	0.77	0.71	0.85	1.00
2024	0.87	0.83	0.89	0.82	0.44	0.64	0.85	0.85	1.00	1.00	1.00	0.95	1.00	1.00	1.00	1.00

The classification accuracy, including Overall Accuracy (OA), kappa coefficient, Producer Accuracy (PA), and User Accuracy (UA), is summarized in Table 2.

3.2.2 Runoff calculation using the SCS-CN method

Runoff was estimated using the Soil Conservation Service Number (SCS-CN) method, which relates precipitation, land cover, and soil type to runoff generation. Soil texture data from "OpenLandMap" were used to determine four hydrologic soil groups (HSG), affecting infiltration rates. Curve number (CN) values were assigned based on land cover and soil group, then adjusted for antecedent moisture conditions (AMC: I – dry condition with five-day antecedent rain less than 13 mm; II – average when AMC is greater than or equal to 13 mm and less than 28 mm; III – wet condition with AMC more than 28 mm). AMC II CN was based on a combination of LULC and soil group conditions [33], and CNs for AMC I and III were calculated using Equations (1) and (2) following a previous study [33].

$$CN(I) = CN(II)/(2.281 - 0.0128\,CN(II)) \quad (1)$$

$$CN(III) = CN(II)/(0.427 - 0.00573\,CN(II)) \quad (2)$$

The CN was used to calculate maximum retention, S, using Equation (3) [33].

$$S = (25400/CN) - 254 \quad (3)$$

The predicted runoff, Q, was calculated using the following SCS-CN Equation (4) [33].

$$Q = (P - 0.2\,S)^2/(P + 0.8S) \quad \text{for } P > 0.2S \quad (4)$$

where P is the precipitation from the Climate Hazards Group InfraRed Precipitation with Station (CHIRPS), providing long-term (2000 – present) and high spatial resolution (500 m), and S is the possible maximum retention. Runoff occurs when rainfall exceeds 20% of possible retention; alternatively, if $P \leq 0.2$, the precipitation is entirely absorbed by the soil, and there is no runoff. This equation, therefore, incorporates the link between rainfall and land cover into a physically based runoff estimate.

The water budget equation is the general equation giving a relationship between precipitation (P) as inputs, MODIS evapotranspiration (ET) and runoff (Q) as outputs, and change in storage (ΔS) as given in Equation (5) [34, 35].

$$P - Q - ET \pm \Delta S = 0 \quad (5)$$

The individual contribution of every land cover class to storage and runoff was determined by way of an area-weighted calculation, in which the average runoff or storage value per land cover class was multiplied by its relative area in proportion to the total catchment area. The resultant percentages indicated the relative contribution of every land cover class to the overall hydrological response.

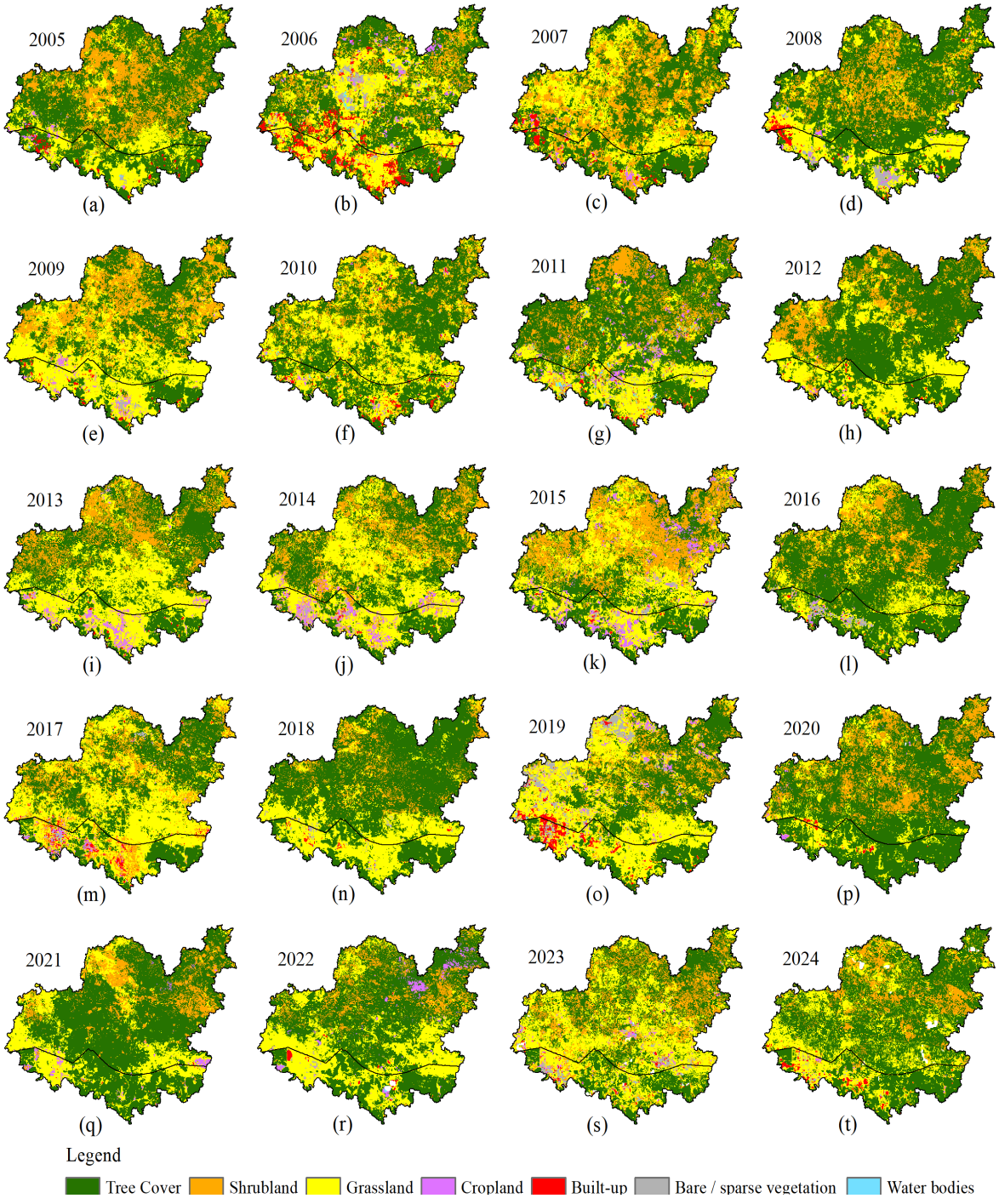

Fig. 4. Spatiotemporal land cover over the study area from (a) 2005 to (t) 2024 on an annual scale

3.2.3 Moisture stress and vegetation health analysis

The Moisture Stress Index (MSI) was derived from MODIS data to quantify plant moisture stress. Cloud and shadow pixels were masked, and MSI was calculated as the ratio of SWIR to NIR bands [36, 37]. The Enhanced Vegetation Index (EVI) from MODIS was used to assess vegetation health. Monthly analysis was performed for vegetation types between 2005 and 2024 to monitor vegetation dynamics regarding runoff and storage changes.

4. RESULTS

4.1 Spatiotemporal Land Cover Changes

The spatial patterns of land cover varied annually, as presented in Figure 4. Tree cover is present in the protected areas only (the northern region of the study site), but in 2015 declined sharply and was transformed into shrubland, grassland, and bareland. This was a result of the long dry season, coupled with

the widespread extent of burning. The same conditions also existed in other prolonged dry seasons, including 2006, 2009, 2019, and 2023, but not as severely as during 2015. The developed area within the cultivation area (southern section of the study area) shows that there are small huts where local people reside for accommodation purposes as they practice farming.

Tree cover experienced significant fluctuation, declining 7,294 ha in 2005 to 4,547 ha in 2009 and increasing again until 2012 (7,475 ha) as shown in Figure 5. In 2015 and 2019, tree cover considerably decreased, likely due to forest fires or deforestation, reaching 3,932 ha and 4,704 ha, respectively. This drastic decrease was most. Shrubland generally decreased over time but saw spikes in 2007, 2015, and 2023, likely linked to disturbance and post-fire vegetation regeneration. Grassland demonstrated dynamic changes, peaking in 2019 (5,518 ha). Cropland area was generally small |but fluctuated sharply, with a peak in 2015, followed by a decrease. Built-up area peaked in 2006 and remained relatively stable. Bare or sparse vegetation cover showed large spikes in fire years (2015, 2019), then decreased.

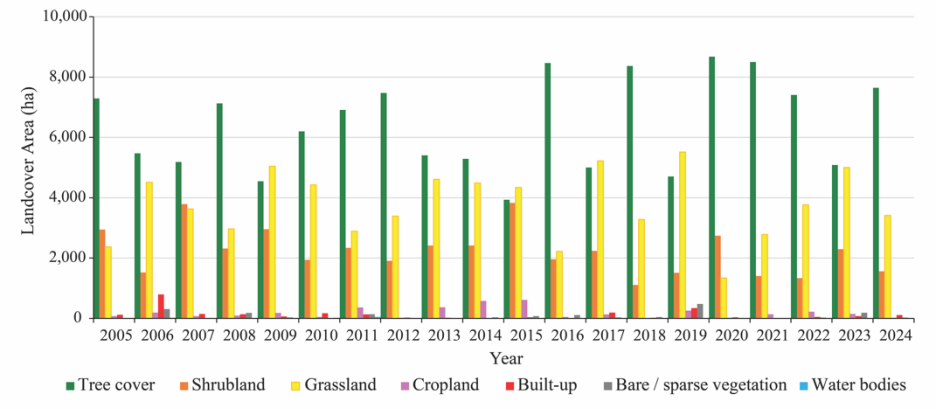

Fig. 5. Trends of land cover changes in the study area from 2005 to 2024 on an annual scale

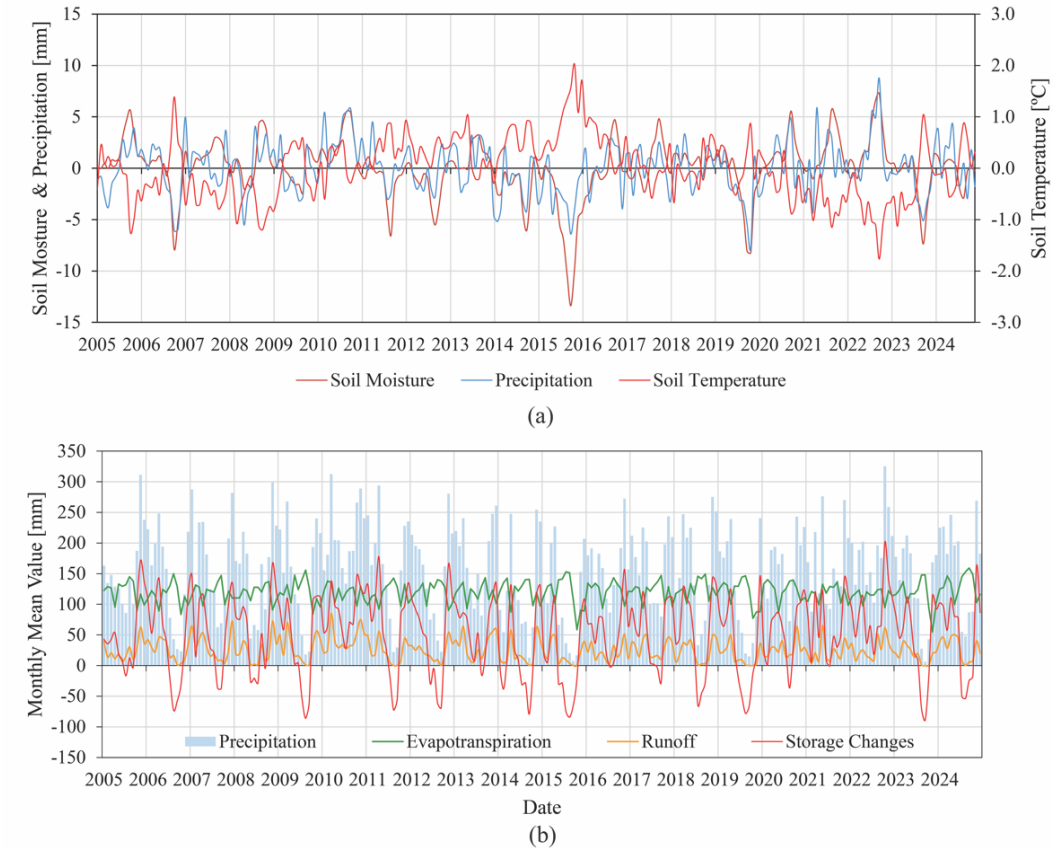

Fig. 6. Time series of (a) precipitation, soil moisture, and soil temperature anomaly and (b) water balance components from 2005 to 2024

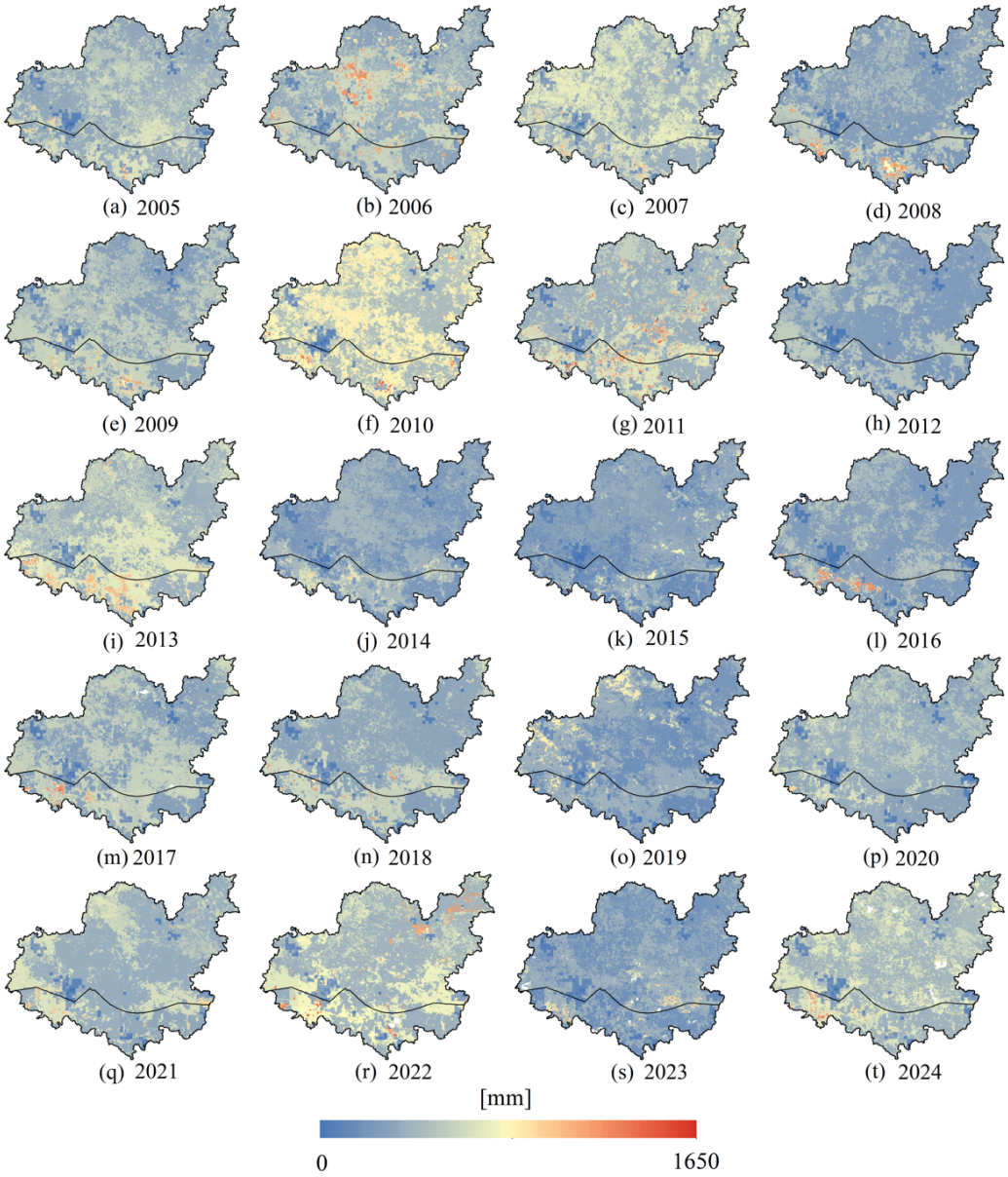

Fig. 7. Spatiotemporal runoff in the study area from (a) 2005 to (t) 2024 on an annual scale

4.2 Climate and Water Balance

Climate and hydrology dynamics were analyzed through precipitation anomalies, soil moisture, and soil temperature from 2005 to 2024 (Figure 6a). Precipitation anomalies were highly variable, with wet years like 2010, 2016, 2021, and 2022 (La Niña) and severe drought in 2015 (El Niño). This intimate link would imply that water storage within the peatland would be in direct control of rainfall variation, especially during extended wet or dry seasons.

Soil moisture anomalies closely followed precipitation, with the highest in 2010 and the lowest in 2015. Fluctuations of soil temperature anomaly followed those of rainfall and soil moisture, but in an inverse relationship, with the anomaly peaking in 2015. Water balance components (Figure 6b) demonstrated higher precipitation and surpluses in 2010 and 2022, as indicated by the positive change in water storage. While El Niño years (2015, 2019, 2023) led to considerable deficits. Trends reflected the close relation between climatic variability and hydrological response. The relation shows El Niño–La Niña cycles dominating long-term water supply and thermal regime in the research area. In addition, the prolonged negative water balance of the subsequent years of drought supported the cumulative stress potential to peatland hydrology. Such prolonged deficits could exacerbate land degradation and accelerate the susceptibility of the peat surface to wildfire under prolonged droughts.

4.3 Spatiotemporal Runoff Variation

Runoff varied spatially throughout the study period (Figure 7). Red indicates high runoff, blue low. Lower runoff values occurred during El Niño years (2014, 2015, 2018, 2019, and 2023), as expected with low precipitation. The highest runoff occurred in 2010, linked to the La Niña. In 2008, 2012, and 2016, low runoff occurred despite high precipitation, except in agricultural areas. This lower runoff in conservation zones suggests land cover slowed runoff and enhanced soil infiltration.

Broader high runoff occurred in 2007 and 2017, related to El Niño impacts in previous years (2006, 2015), particularly in agricultural areas. Moderate runoff appeared in both the cultivation and conservation regions, especially near the border between the two regions, peaking in 2022 after the 2015 El Niño, and similarly in 2024 after the 2023 El Niño. This is likely due to the moderate dry season in 2019 and 2023, contributing to tree cover degradation.

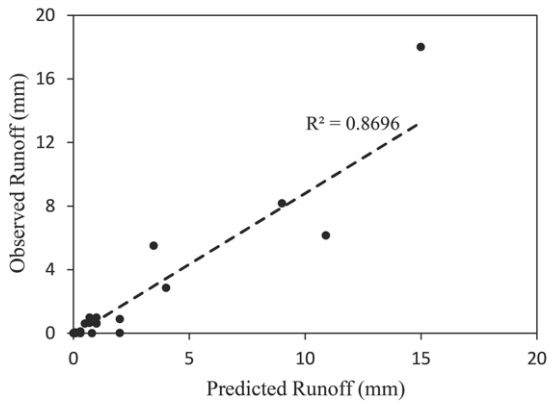

Fig. 8. Correlation between observed and predicted runoff

Oil palm and rubber plantations (classified as tree cover) in the southern cultivation area consistently showed low runoff. It should be noted that the tree cover class, adopted from the ESA WorldCover classification, included both natural peat swamp forest and managed plantations. Such generalization might partially account for the relatively low runoff values obtained for this class since hydrological responses between natural forests and plantations varies due to differences in rooting systems and soil compaction. However, having a standardized classification introduces consistency into spatial and temporal analyses and does not introduce bias by manual reclassification.

High runoff was observed outside the plantation areas during El Niño events (e.g., 2007–2009, 2016–2018, and 2020–2022), and sometimes in conservation areas near cultivation borders, especially in 2023, likely from land cover damage. The model showed good performance (runoff observation vs. prediction correlation = 0.87, and the Nash–Sutcliffe efficiency (NSE) = 0.89; Figure 8).

4.4 Spatiotemporal Water Storage Changes

Changes in water storage in the study area from 2005 to 2024 were estimated, indicating hydrological dynamics (Figure 9). A positive water storage change means surplus, and a negative means a deficit. The average annual water deficit was -106.41 mm, peaking at -305.53 mm in 2015 (extreme El Niño drought). Variability was high (SD ±91.73 mm), and over half of the years experienced significant deficits (median -109.05 mm). Average surplus was 697.87 mm, highest in 2010 (1058.62 mm, La Niña) and lowest in 2006 (262.55 mm), with large fluctuations (SD ±193.65 mm).

Annual storage change averaged 591.46 mm (SD ±263.08 mm), highest in 2010 (surplus only), and lowest in 2015 (large deficit). Trends showed increase in deficits during El Niño years (e.g., 2006, 2009, 2015, 2019, and 2023), mainly in degraded areas, likely from climate pressures and land use changes (agriculture, canalization, illegal logging). Degraded areas were mostly located around boundaries of conservation and cultivation (Rawa Tanam, Rambai, Perigi, Bukit Batu). Surplus patterns closely followed annual climate variability, spiking in wet years (2010 and 2022). Deficit and surplus were moderately negatively correlated (-0.65), while deficit and storage change were strongly negatively correlated (-0.83). Surplus and storage change were highly positively correlated (+0.96), indicating rainfall's crucial influence on water balance.

4.5 Runoff Variations in Land Cover Types

Each land cover's contribution to runoff was analyzed (2005 to 2024). Bare/sparse vegetation contributed most to runoff (avg. 29%, SD 14.15%), peaking at 48% in 2020 (Figure 10), linked to peatland fires or massive land clearing in 2019. Cropland contribution to runoff averaged 26.45%, spiking in 2018 (58%, 148.39 mm) due to intensive agriculture, also high in 2010 (32%, 131.20 mm).

Built-up areas had lower contributions (avg. 14.85%) since structures were semi-permanent in the form of small stilt houses made of bamboo or wood, used by farmers as shelters, and allowed infiltration, unlike urban areas. Tree cover had the lowest runoff contribution (avg. 6.6%), with the lowest values in 2020 (4%) and 2018 (3%), which were better periods for tree cover to reduce runoff. Shrubs and grassland contributed moderately (10.3% and 11.8%); shrubs retained water better due to deeper roots.

Overall (Figure 11a), tree cover contributed the lowest runoff value (7%) and the highest storage change (31%), reflecting its essential role in

absorbing rainwater and retaining soil moisture. Bare or sparse vegetation had the highest runoff (29%) and the lowest storage change (1%), indicating hydrological degradation.

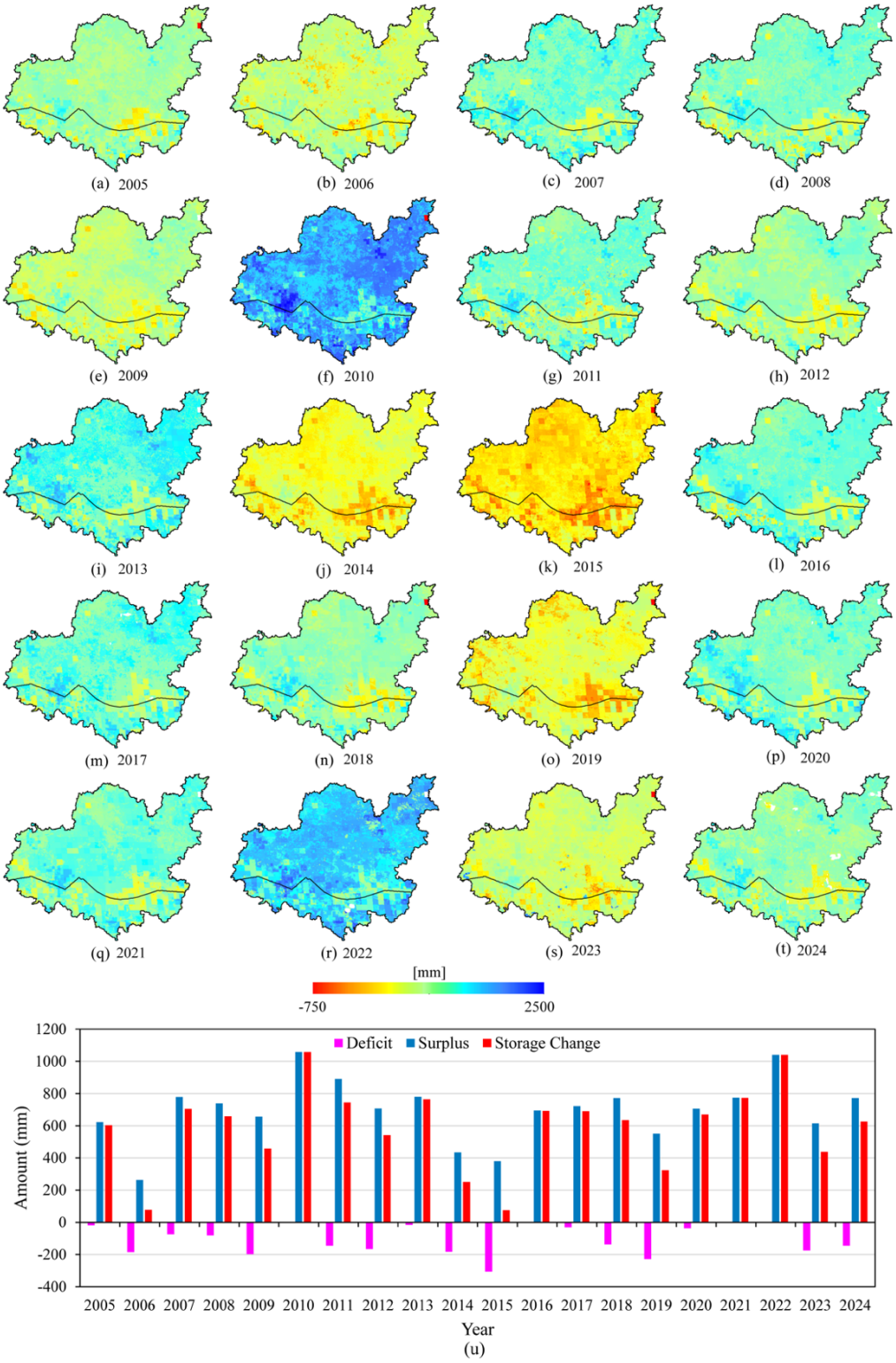

Fig. 9. Maps of the storage changes in the study area from (a) 2005 to (t) 2024 and trends of the deficit, surplus, and total storage change (u) on an annual scale

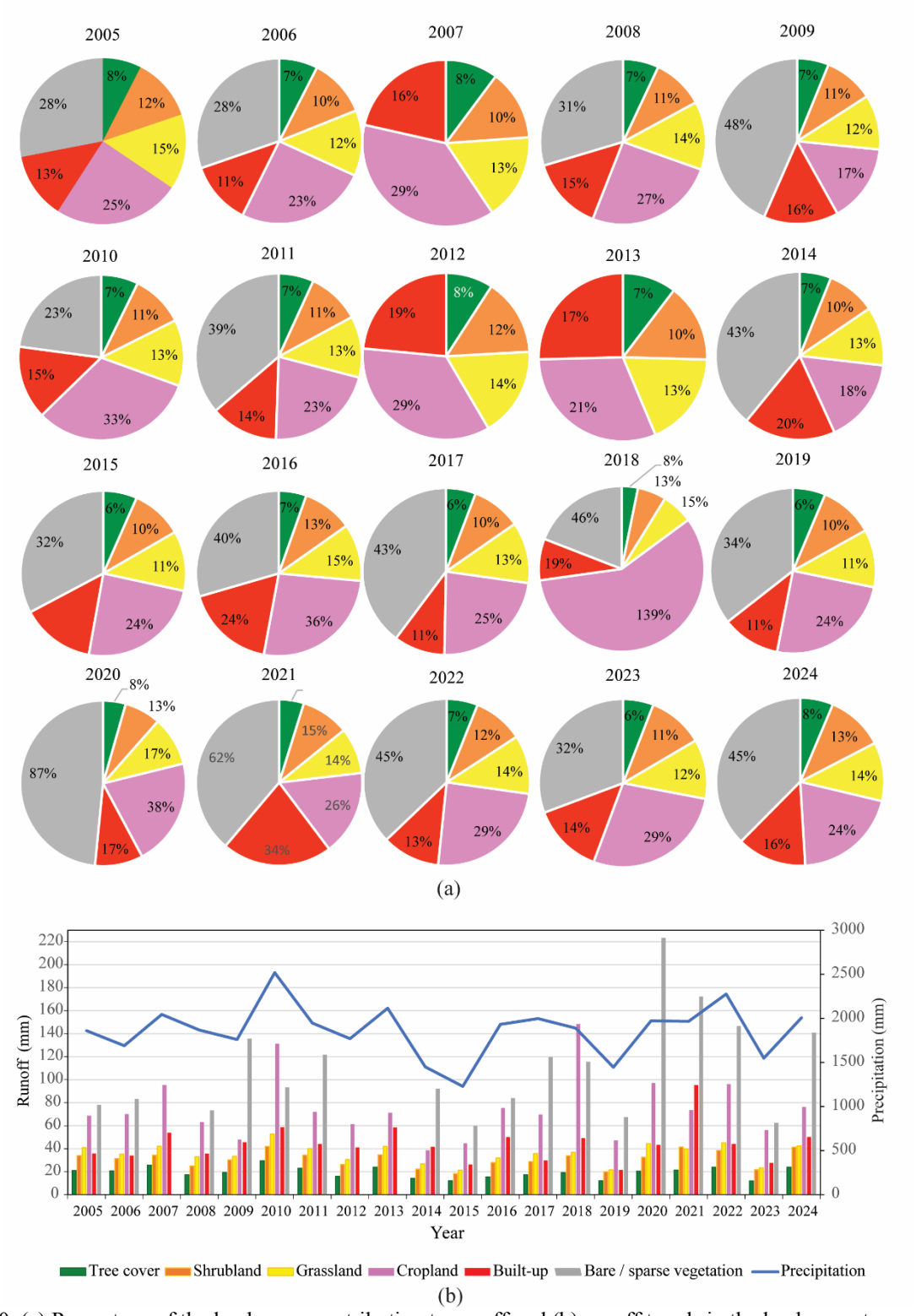

Fig. 10. (a) Percentage of the land cover contribution to runoff and (b) runoff trends in the land cover types

Runoff and storage change were highly negatively correlated (-0.98) as presented in Figure 11b. This negative correlation is a sign of opposing hydrology processes supplied by tree cover and degraded land. Tree cover enhances water infiltration and storage as well as open soil, facilitating surface flow. The values of shrublands and croplands were intermediate and indicate a poor ability to store water as a function of canopy cover and crop cycle. This implies that land cover change can greatly modify peat hydrology by adjusting the ratio of infiltration and runoff. This is one of the reasons why restoration of forest cover is critical in ensuring long-term water supply during dry weather.

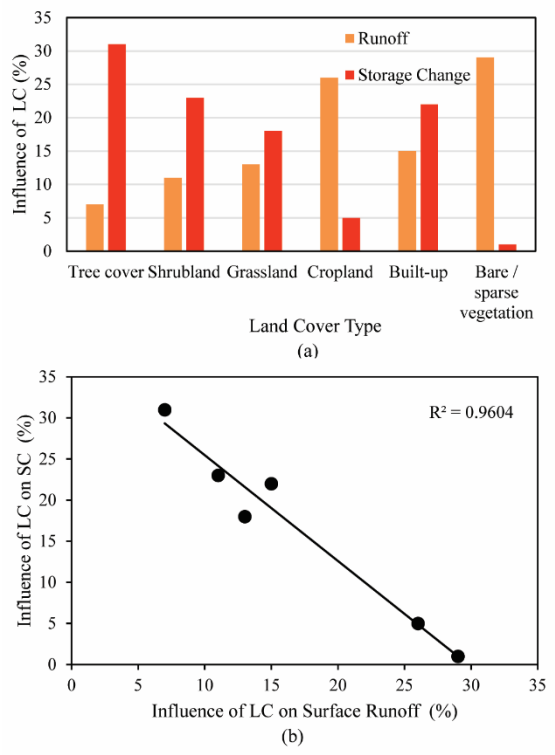

Fig. 11. (a) Influence of land cover (LC) types on surface runoff and storage changes, and (b) correlation between land cover influences on runoff (%) and storage change (%)

4.6 Impact of Drought on Vegetation Health

To assess drought impacts on vegetation, monthly average MSI and EVI from 2015 to 2024 were mapped (Figure 12). High MSI (moisture stress) and low EVI (vegetation health) mainly occurred in the cultivated area, the southern part of the study area, with intensive canalization for plantation and agriculture. Most conservation areas had lower MSI and higher EVI, indicating better moisture for vegetation health and better water resource management.

Low EVI and high MSI varied by land cover (Figure 13), peaking in drought years (2006, 2009, 2015, 2019, 2023). Trees cover and shrubland had higher EVI and lower MSI than grassland and cropland. Interestingly, the shrubland slightly outperformed tree cover during droughts, suggesting greater resilience. Cropland had low EVI and high MSI, indicating high sensitivity to moisture changes.

5. DISCUSSION

In the study area, fires and land conversion led to a sharp drop in tree cover in drought years. Such trends are typical in Southeast Asian tropical peatlands that burn during prolonged dry season, triggered by El Niño, and peatland conversion to oil palm plantations or agriculture [38]. Meanwhile, shrub and grassland increased, suggesting secondary regeneration after disturbance. In the Amazon region, secondary vegetation also grew after disturbances such as forest fires [39]. The detection of secondary vegetation is possible due to the loss of tree cover that exposes underlying shrubs and grasses. After deforestation, remote sensing can detect land cover changes, including shrub and grassland.

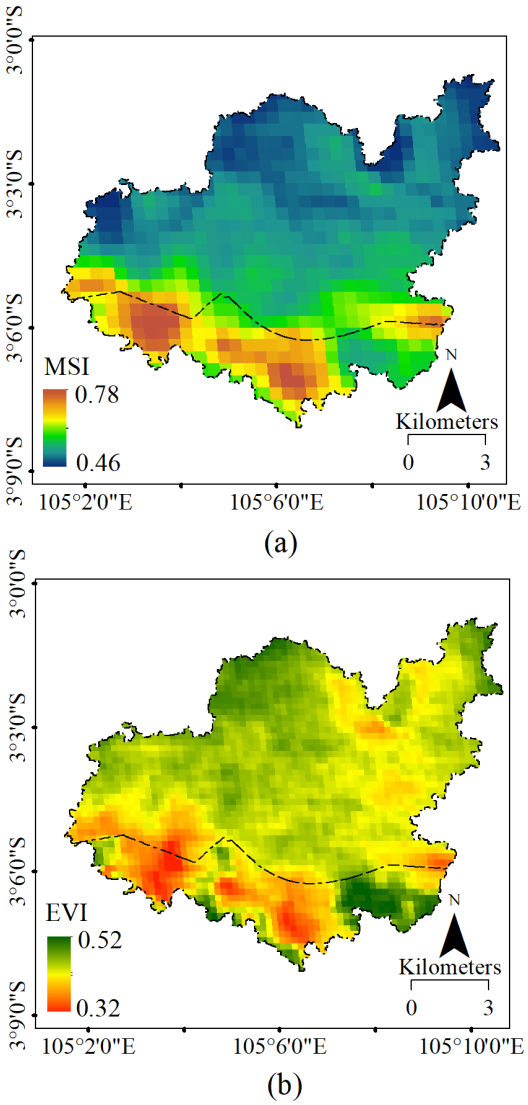

Fig. 12. Monthly mean MSI and EVI for the period of 2005 – 2024

Hydrological conditions were influenced by rainfall variation. The most severe water deficit occurred in 2015 due to minimal rainfall and a long dry season caused by the El Niño. Conversely, the largest water surplus occurred in 2010, primarily due to the La Niña. Thus, hydrological conditions in the study area were closely tied to climate. In addition to climate, extensive canalization for plantations and agriculture exacerbated drought and water deficits. Drainage canals doubled drought intensity in several peat areas, such as the Kampar Peninsula, Air Hitam,

and Air Sugihan in Sumatra, as well as Sebangau Forest, Upper Kapuas, and Kutai Peatlands in Kalimantan [40]. Conversion of peatlands to plantations increased drought severity by up to four times. Hence, peatland hydrology was significantly influenced by natural factors and human activities, particularly through changes in land cover.

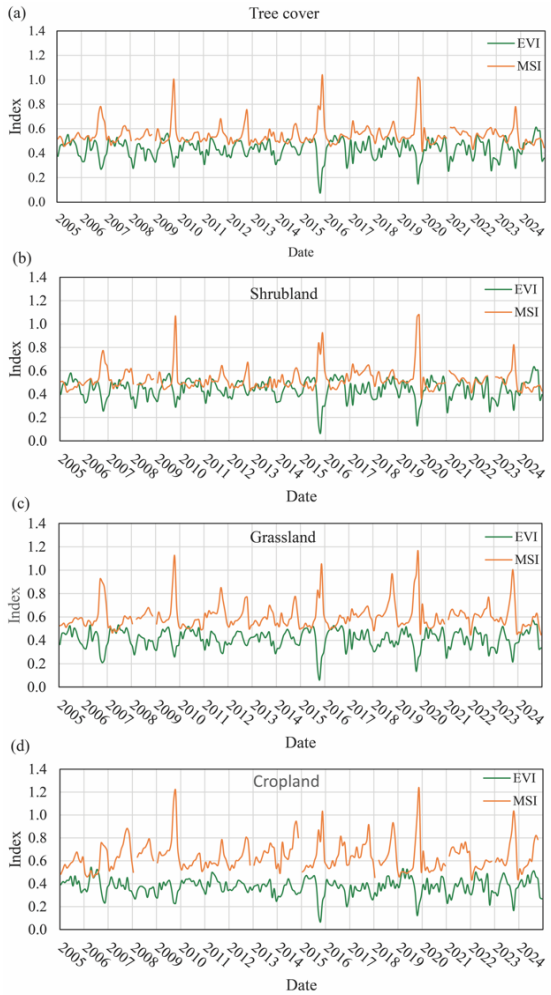

Fig. 13. MSI and EVI for four land cover categories

Land cover influences hydrology through its impact on runoff. Modelling shows that tree cover had the lowest contribution to runoff. During high rainfall, areas with tree cover experienced the largest surplus, influencing storage change by 31% of the total land cover. In contrast, agricultural land increased surface runoff, indicating reduced water infiltration capacity. Previous studies found that massive canalisation in farming areas increased the tendency for water to flow through canals instead of infiltrating peat [1, 31].

Previous investigations were also conducted in other Indonesian peatland watersheds through physically based hydrological models like SWAT and HEC-HMS [41–43]. Even though the study did not give explicit quantitative volumes of runoff, their findings showed comparable hydrological tendencies to the results yielded from the SCS-CN method applied through this study. For example, canal blocking successfully decreased surface runoff and improved groundwater storage [41], and in the Kahayan–Sebangau peat hydrological unit improved water storage and decreased flow concentration [42]. Flood peaks were higher in disturbed peat catchments as suggested by HEC-HMS simulations [43]. These are consistent with the results obtained now, where bare and degraded lands generated the highest runoff, whereas tree-covered areas produced the lowest runoff. Even though direct numerical comparison is not possible, the consistency of runoff behavior for all types of land use guarantees the validity and reliability of the modelled results.

Hydrological restoration through canal blocking for rewetting increased the water level and moisture in the peat. This approach also increased peat water content in the Mega Rice Project area, Central Kalimantan [44]. Vegetation health indices (MSI, EVI) indicated high drought stress on agricultural land, as shown by high MSI and low EVI values. Shrubs were more resilient to drought than other land cover types, suggesting their importance during the transition stage of post-disturbance peat restoration, alongside the growth of secondary trees.

Although restoration activities have been conducted in the study area, these activities were mostly regulatory and hydrologically focused on preventing land burning and increasing peat moisture through canals blocking. Revegetation at high densities has not been widely implemented, since tree planting was in small areas and therefore could not be detected by medium-resolution satellite imagery like Landsat-7 and Landsat-8. Therefore, tree cover increase and hydrological enhancement are considered here as indirect responses to restoration measures that reduced fire recurrence and protected soil moisture, rather than as direct consequences of broad-scale reforestation.

The SCS-CN model is a robust empirical solution and a realistic model for predicting surface runoff. Nevertheless, its simplicity is its weakness. The CN tables were originally developed for mineral soils and may not fully represent peatland hydrological behavior, which is influenced by extreme water retention, macropore flow, and artificial drainage. It does not account for groundwater table dynamics and lateral subsurface flow explicitly, which are quite significant in terms of their impact on peatland hydrology, moisture budget, and fire risk. As such, the outcomes discussed herein must be understood as surface-level hydrologic response, rather than a full description of the groundwater system. Further, the change in storage was represented as a residual term of the water balance equation. It is reacting responsively to uncertainty in the input terms, i.e., precipitation, runoff, and evapotranspiration. Absent independent verification against groundwater level measurements, the storage changes should be viewed

as indicative estimates that approximate overall trends in storage instead of absolute values. However, the consistent temporal behavior between the storage changes and the rainfall anomalies indicates that the residual approach satisfactorily describes large-scale fluctuations in storage in the peatland system.

6. CONCLUSION

This study provides an analysis of the cover dynamics, surface runoff, and water storage within Sugihan–Saleh River Peat Hydrological Unit, South Sumatra, from 2005 to 2024. Multi-temporal images of Landsat-7 and Landsat-8 have presented profound changes in tree cover reduction inside this hydrological. Climatic variability strongly controls precipitation through El Niño and La Niña episodes, thus controlling soil moisture content as well as soil temperature. Direct anomalies in soil moisture responding to rainfall variance have proven the high sensitivity of peatland hydrology toward climatic fluctuations.

Runoff analysis showed that bare or lightly vegetated grounds generated the greatest runoff, and tree-covered grounds generated the minimum runoff. Seasonal storage fluctuations of water revealed excesses during wet periods and extreme deficits during dry periods, particularly in El Niño events. Tree-dominated peatlands and reserved peatlands had greater soil saturation, reduced water stress, and healthier vegetation compared with cropped land, which suggests the crucial role of such peatlands in hydrological stability and minimization of drought risk.

Restoration of the study area of peatlands has leaned more towards hydrological control and prevention from fires through canal blocking and less towards massive afforestation. The SCS-CN approach used here provides a good empirical model for the estimation of surface runoff, but cannot fully obtain subsurface flow or groundwater change. The results should therefore be interpreted as indicative hydrological patterns rather than quantitative findings.

7. ACKNOWLEDGMENTS

We would like to acknowledge *Direktorat Riset, Teknologi, dan Pengabdian kepada Masyarakat* (DRTPM) for financial support through "*Penelitian Fundamental Reguler*", Contract Number: 090/E5/PG.02.00.PL/2024, dated 5 July 2023. We also thank anonymous reviewers and the academic editor for their valuable comments and suggestions.

8. REFERENCES

[1] Khakim M. Y. N., Bama A. A., and Tsuji T., Spatiotemporal Variations of Soil Moisture and Groundwater Level in a South Sumatra Peatland, Indonesia During 2015–2018, Geography, Environment, Sustainability, Vol. 15, No. 2, 2022, pp.58–70. https://doi.org/10.24057/2071-9388-2021-137

[2] Yuwati T. W., Rachmanadi D., Pratiwi Turjaman M., Indrajaya Y., Nugroho H. Y. S. H., Qirom M. A., Narendra B. H., Winarno B., Lestari S., Santosa P. B., Adi R. N., Savitri E., Putra P. B., Wahyuningtyas R. S., Prayudyaningsih R., Halwany W., Nasrul B., Bastoni, and Mendham D., Restoration of degraded tropical peatland in indonesia: A review, Land, Vol. 10, No. 11, 2021, pp.1–31. doi:10.3390/land10111170

[3] Basuki I., Kauffman J. B., Peterson J. T., Anshari G. Z., and Murdiyarso D., Land Cover and Land Use Change Decreases Net Ecosystem Production in Tropical Peatlands of West Kalimantan, Indonesia, Forests, Vol. 12, No. 11, 2021, 1587. doi:10.3390/f12111587

[4] International Energy Agency (IEA), Kementerian Energi dan Sumber Daya Mineral Republik Indonesia (MEMR), An Energy Sector Roadmap to Net Zero Emissions in Indonesia, Paris, 2022. https://www.iea.org/reports/an-energy-sector-roadmap-to-net-zero-emissions-in-indonesia

[5] Harenda K. M., Lamentowicz M., Samson M., and Chojnicki B. H., The Role of Peatlands and Their Carbon Storage Function in the Context of Climate Change, 2018, pp.169–187. https://doi.org/10.1007/978-3-319-71788-3_12

[6] Cuthbert M. O., Gleeson T., Moosdorf N., Befus K. M., Schneider A., Hartmann J., and Lehner B., Global patterns and dynamics of climate–groundwater interactions, Nature Climate Change, Vol. 9, No. 2, 2019, pp.137–141. https://doi.org/10.1038/s41558-018-0386-4

[7] Leng L. Y., Ahmed O. H., and Jalloh M. B., Brief review on climate change and tropical peatlands, Geoscience Frontiers, Vol. 10, No. 2, 2019, pp.373–380. https://doi.org/10.1016/j.gsf.2017.12.018

[8] Setyawati W., and Suwarsono, Carbon Emission from Peat Fire in 2015, IOP Conference Series: Earth and Environmental Science, Vol. 166, 2018, 012041. https://doi.org/10.1088/1755-1315/166/1/012041

[9] Lin S., Liu Y., and Huang X., Climate-induced Arctic-boreal peatland fire and carbon loss in the 21st century, Science of The Total Environment, Vol. 796, 2021, 148924. https://doi.org/10.1016/j.scitotenv.2021.148924

[10] Azmi N. A. C., Apandi N. M., and Rashid A. S. A., Carbon emissions from the peat fire problem—a review, Environmental Science and Pollution Research, Vol. 28, No. 14, 2021, pp.16948–16961. https://doi.org/10.1007/s11356-021-12886-x

[11] Hein L., Spadaro J. V., Ostro B., Hammer M., Sumarga E., Salmayenti R., Boer R., Tata H., Atmoko D., Castañeda J. P., The health impacts of Indonesian peatland fires, Environmental Health, Vol. 21, No. 62, 2022. https://doi.org/10.1186/s12940-022-00872-w

[12] Czapiewski S., and Szumińska D., An overview of remote sensing data applications in peatland research based on works from the period 2010–2021, Land, Vol. 11, No. 1, 2022. https://doi.org/10.3390/land11010024

[13] Lee H., Yuan T., Yu H., and Jung H. C., Interferometric SAR for Wetland Hydrology: An Overview of Methods, Challenges, and Trends, IEEE Geoscience and Remote Sensing Magazine, Vol. 8, No. 1, 2020, pp.120–135. https://doi.org/10.1109/MGRS.2019.2958653

[14] Benscoter B. W., Thompson D. K., Waddington J. M., Flannigan M. D., Wotton B. M., De Groot W. J., and Turetsky M. R., Interactive effects of vegetation, soil moisture and bulk density on depth of burning of thick organic soils, International Journal of Wildland Fire, Vol. 20, No. 3, 2011, pp.418–429. https://doi.org/10.1071/WF08183

[15] Taufik M., Veldhuizen A. A., Wösten J. H. M., and van Lanen H. A. J., Exploration of the importance of physical properties of Indonesian peatlands to assess critical groundwater table depths, associated drought and fire hazard, Geoderma, Vol. 347, 2019, pp.160–169. https://doi.org/10.1016/j.geoderma.2019.04.001

[16] Garkusha I. N., Hnatushenko V. V., and Vasyliev V. V., Using Sentinel-1 data for monitoring of soil moisture, International Geoscience and Remote Sensing Symposium (IGARSS), 2017, pp.1656–1659. https://doi.org/10.1109/IGARSS.2017.8127291

[17] Mohanty B. P., Cosh M. H., Lakshmi V., and Montzka C., Soil moisture remote sensing: State-of-the-science, Vadose Zone Journal, Vol. 16, No. 1, 2017. https://doi.org/10.2136/vzj2016.10.0105

[18] Dadap N. C., Cobb A. R., Hoyt A. M., Harvey C. F., and Konings A. G., Satellite soil moisture observations predict burned area in Southeast Asian peatlands, Environmental Research Letters, Vol. 14, No. 9, 2019. https://doi.org/10.1088/1748-9326/ab3891

[19] Luscombe D. J., Anderson K., Grand-Clement E., Gatis N., Ashe J., Benaud P., Smith D., and Brazier R. E., How does drainage alter the hydrology of shallow degraded peatlands across multiple spatial scales?, Journal of Hydrology, Vol. 541, 2016, pp.1329–1339. https://doi.org/10.1016/j.jhydrol.2016.08.037

[20] Evers S., Yule C. M., Padfield R., O'Reilly P., and Varkkey H., Keep wetlands wet: the myth of sustainable development of tropical peatlands – implications for policies and management, Global Change Biology, Vol. 23, No. 2, 2017, pp.534–549. https://doi.org/10.1111/gcb.13422

[21] President of Republic of Indonesia. Peat Restoration Agency, Pub. L. No. 1, 2016, Indonesia

[22] Chathuranika I. M., Gunathilake M. B., Baddewela P. K., Sachinthanie E., Babel M. S., Shrestha S., Jha M. K., and Rathnayake U. S., Comparison of Two Hydrological Models, HEC-HMS and SWAT in Runoff Estimation: Application to Huai Bang Sai Tropical Watershed, Thailand, Fluids, Vol. 7, No. 8, 2022, 267. https://doi.org/10.3390/fluids7080267

[23] Jawad A. A., Hassan W. H., and Fattah M. Y., Numerical analysis of a zoned earth dam considering hydrodynamic force during the earthquake excitation, Journal of Physics: Conference Series, Vol. 1973, No. 1, 012183. 2021. doi:10.1088/1742-6596/1973/1/012183

[24] Mohamed M., Karim I., and Fattah M., Impact of Dam Materials and Hydraulic Properties on Developing the Breaching Dimensions, *Engineering and Technology Journal*, Vol. 41, No. 5, 2023, pp.716–723. doi:10.30684/etj.2023.138009.1368

[25] Mohamed M. J., Karim I. R., Fattah M. Y., and Al-Ansari N., Modelling Flood Wave Propagation as a Result of Dam Piping Failure Using 2D-HEC-RAS, Civil Engineering Journal, Vol. 9, No. 10, 2023, pp.2503–2515. doi:10.28991/CEJ-2023-09-10-010

[26] Singh H., Alam M. A., Sharma P. J., and Rautela K. S. (2023). A comparison of the SCS-CN-based models for hydrological simulation of the Aghanashini River, Karnataka, India, AQUA — Water Infrastructure, Ecosystems and Society, Vol. 72, No. 4, pp.507–519. https://doi.org/10.2166/aqua.2023.213

[27] Tañagras J., Macuha1 R., and Herrera E., Impact Evaluation of Land Use–Land Cover Change on the Hydrology of Salipit River Basin Cavite, Philippines, International Journal of GEOMATE, Vol. 25, No. 110, 2023, pp. 140–147. doi:10.21660/2023.110.3852

[28] Soulis K. X., Soil conservation service curve number (SCS-CN) method: Current applications, remaining challenges, and future perspectives, Water (Switzerland), Vol. 13, No. 2, 2021. https://doi.org/10.3390/w13020192

[29] Mishra S. K., and Singh V. P. (2003). SCS-CN Method, Soil Conservation Service Curve Number (SCS-CN) Methodology. Water Science and Technology Library (Vol. 42), Springer, Dordrecht, pp.84–146. https://doi.org/10.1007/978-94-017-0147-1_2

[30] Rawat K. S., Singh S. K., and Szilard S., Comparative evaluation of models to estimate direct runoff volume from an agricultural watershed, Geology, Ecology, and Landscapes, Vol. 5, No. 2, 2021, pp.94–108. https://doi.org/10.1080/24749508.2020.1833629

[31] Khakim M. Y. N., Bama A. A., Yustian I., Poerwono P., Tsuji T., and Matsuoka T. Peatland subsidence and vegetation cover degradation as impacts of the 2015 El niño event revealed by Sentinel-1A SAR data, International Journal of Applied Earth Observation and Geoinformation, Vol. 84, 2020, 101953. https://doi.org/10.1016/j.jag.2019.101953

[32] Zanaga D., Van De Kerchove R., De Keersmaecker W., Souverijns N., Brockmann C., Quast R., Wevers J., Grosu A., Lang S., Tsendbazar N. E., Li L., Tarko A., Waeber M., Bartsch A., and Smets B., ESA WorldCover 10 m 2021 v200, 2022. https://doi.org/10.5281/zenodo.7254221

[33] Jain S., Jaiswal R. K., Lohani A. K., and Galkate R., Development of cloud-based rainfall-run-off model using Google Earth Engine, Current Science, Vol. 121, No. 11, 2021, pp.1433–1440.

[34] Healy R. W., Winter T. C., LaBaugh J. W., and Franke O. L., Water Budgets: Foundations for Effective Water-Resources and Environmental Management, 2007. https://doi.org/10.3133/cir1308

[35] Amindin A., Siamian N., Dereimi Z. N., Clague J. J., Blaschke T., and Pourghasemi H. R., Long term analysis of international wetlands in Iran: Monitoring surface water area and water balance, International Journal of Applied Earth Observation and Geoinformation, Vol. 126, 2024, 103637. https://doi.org/10.1016/j.jag.2023.103637

[36] Braga P., Crusiol L. G. T., Nanni M. R., Caranhato A. L. H., Fuhrmann M. B., Nepomuceno A. L., Neumaier N., Farias J. R. B., Koltun A., Gonçalves L. S. A., and Mertz-Henning L. M., Vegetation indices and NIR-SWIR spectral bands as a phenotyping tool for water status determination in soybean, Precision Agriculture, Vol. 22, No. 1, 2021, pp.249–266. https://doi.org/10.1007/s11119-020-09740-4

[37] Hunt Jr E., and Rock B., Detection of changes in leaf water content using Near- and Middle-Infrared reflectances☆, Remote Sensing of Environment, Vol. 30, No. 1, 1989, pp.43–54. https://doi.org/10.1016/0034-4257(89)90046-1

[38] Miettinen J., Hooijer A., Wang J., Shi C., and Liew S. C., Peatland degradation and conversion sequences and interrelations in Sumatra, Regional Environmental Change, Vol. 12, No. 4, 2012, pp.729–737. https://doi.org/10.1007/s10113-012-0290-9

[39] Aragão L. E. O. C., Anderson L. O., Fonseca M. G., Rosan T. M., and Vedovato L. B., 21st Century drought-related fires counteract the decline of Amazon deforestation carbon emissions, Nature Communications, Vol. 9, No. 536, (2018). https://doi.org/10.1038/s41467-017-02771-y

[40] Taufik M., Minasny B., McBratney A. B., Van Dam J. C., Jones P. D., and Van Lanen H. A. J., Human-induced changes in Indonesian peatlands increase drought severity, Environmental Research Letters, Vol. 15, No. 8, 2020, 084013. https://doi.org/10.1088/1748-9326/ab96d4

[41] Suharnoto Y., Taufik M., Setiawan B. I., Buchori D., and Dewantara B., Development of Spatial Peatland Fire Danger Index Using Coupled SWAT-MODFLOW Model, Sustainability, Vol. 14, No. 13, 2022, 7632. https://doi.org/10.3390/su14137632

[42] Suryadi Y., Soekarno I., and Humam I. A., Effectiveness Analysis of Canal Blocking in Sub-peatland Hydrological Unit 5 and 6 Kahayan Sebangau, Central Kalimantan, Indonesia, Journal of Engineering and Technological Sciences, Vol. 53, No. 2, 2021, 210205. https://doi.org/10.5614/j.eng.technol.sci.2021.53.2.5

[43] Ikhwali M. F., Pawattana C., Nur S., Azhari B., Ikhsan M., Aida N., and Silvia C. S., Reviews, challenges, and prospects of the application of Hydrologic Engineering Center-Hydrologic Modelling System (HEC-HMS) model in Indonesia, Engineering and Applied Science Research, Vol. 49, No. 5, 2022, pp.669–680. https://ph01.tci-thaijo.org/index.php/easr/article/view/247833

[44] Jaenicke J., Wösten H., Budiman A., and Siegert F., Planning hydrological restoration of peatlands in Indonesia to mitigate carbon dioxide emissions, Mitigation and Adaptation Strategies for Global Change, Vol. 15, No. 3, 2010. pp.223–239. https://doi.org/10.1007/s11027-010-9214-5